THE JOURNAL OF BIOLOGICAL CHEMISTRY VOL. 288, NO. 30, pp. 22128–22140, July 26, 2013

Crystal Structures of Copper-depleted and Copper-bound Fungal Pro-tyrosinase

*INSIGHTS INTO ENDOGENOUS CYSTEINE-DEPENDENT COPPER INCORPORATION**

Received for publication, April 14, 2013, and in revised form, May 29, 2013 Published, JBC Papers in Press, June 7, 2013, DOI 10.1074/jbc.M113.477612

Nobutaka Fujieda[‡], Shintaro Yabuta[‡], Takuya Ikeda[‡], Takuji Oyama[§], Norifumi Muraki[§], Genji Kurisu[§1], and Shinobu Itoh[‡2]

From the [‡]Department of Material and Life Science, Division of Advanced Science and Biotechnology, Graduate School of Engineering, Osaka University, 2-1 Yamada-oka, Suita, Osaka 565-0871 and the [§]Institute for Protein Research, Osaka University, 3-2 Yamada-oka, Suita, Osaka 565-0871, Japan

Background: Fungal tyrosinase maturation involves multiple processes of the dinuclear copper assembly and proteolytic activation.
Results: Structural examinations and mutational studies of the pro-tyrosinases revealed that three endogenous cysteines contribute to the copper incorporation.
Conclusion: The three highly flexible cysteines are essential for assembly of the active site across the protein shell.
Significance: Elucidation of such a copper incorporation process provides useful insights into metal homeostasis.

Tyrosinase, a dinuclear copper monooxygenase/oxidase, plays a crucial role in the melanin pigment biosynthesis. The structure and functions of tyrosinase have so far been studied extensively, but the post-translational maturation process from the pro-form to the active form has been less explored. In this study, we provide the crystal structures of *Aspergillus oryzae* full-length pro-tyrosinase in the holo- and the apo-forms at 1.39 and 2.05 Å resolution, respectively, revealing that Phe[513] on the C-terminal domain is accommodated in the substrate-binding site as a substrate analog to protect the dicopper active site from substrate access (proteolytic cleavage of the C-terminal domain or deformation of the C-terminal domain by acid treatment transforms the pro-tyrosinase to the active enzyme (Fujieda, N., Murata, M., Yabuta, S., Ikeda, T., Shimokawa, C., Nakamura, Y., Hata, Y., and Itoh, S. (2012) *ChemBioChem.* 13, 193–201 and Fujieda, N., Murata, M., Yabuta, S., Ikeda, T., Shimokawa, C., Nakamura, Y., Hata, Yl, and Itoh, S. (2013) *J. Biol. Inorg. Chem.* 18, 19–26). Detailed crystallographic analysis and structure-based mutational studies have shown that the copper incorporation into the active site is governed by three cysteines as follows: Cys[92], which is covalently bound to His[94] via an unusual thioether linkage in the holo-form, and Cys[522] and Cys[525] of the *CXXC* motif located on the C-terminal domain. Molecular mechanisms of the maturation processes of fungal tyrosinase involving the accommodation of the dinuclear copper unit, the post-translational His-Cys thioether cross-linkage formation, and the proteolytic C-terminal cleavage to produce the active tyrosinase have been discussed on the basis of the detailed structural information.

Tyrosinase (EC 1.14.18.1), a dinuclear copper monooxygenase/oxidase, is a key enzyme in the melanin biosynthesis and is widely distributed in mammals, plants, fungi, and bacteria. The dinuclear copper center is involved in the catalytic reactions of tyrosinase, the hydroxylation of phenolic substrates (phenolase activity, Scheme 1), and the subsequent oxidation of catechols to *o*-quinones (catecholase activity, Scheme 1) (1–4). A similar dinuclear copper center, so-called type 3 copper, also plays important roles in catechol oxidase catalyzing exclusively the latter reaction (catecholase activity) and in hemocyanin, which serves as the dioxygen carrier in the hemolymph of mollusks and arthropods (5). In the crystal structures of these proteins, six histidine residues, which are provided by a four-helix bundle in the copper-binding domain, coordinate to the two copper ions (three histidine imidazoles for each copper ion, Cu_A and Cu_B) in the active site (Fig. 1, *A* and *B*) (6–12). In mushroom tyrosinase (12), sweet potato catechol oxidase (8), and octopus hemocyanin (7), one of the histidine imidazole groups coordinating to Cu_A is covalently bound to nearby cysteine via an unusual thioether linkage (Fig. 1), although its function still remains obscure.

In other copper-containing proteins, such as blue copper proteins, multicopper oxidases, cytochrome *c* oxidase, dopamine β-hydroxylase, peptidylglycine α-hydroxylating monooxygenase, particulate methane monooxygenase, quercetin 2,3-dioxygenase, copper amine oxidase, galactose oxidase, and Cu,Zn-SOD, the copper cofactors also play crucial roles to dictate electron transfer, two- and/or four-electron reduction of O_2, alkane hydroxylation, dehydrogenation of alcohols and amines, and superoxide dismutation (13). However, copper is known to be highly toxic to cells due to its undesirable property in yielding the deleterious hydroxyl radical (14). Thus, the copper content inside the cell is severely regulated by copper membrane trans-

* This work was supported in part by Grant-in-aid for Scientific Research on Innovative Areas (Molecular Activation Directed toward Straightforward Synthesis) 22105007 (to S. I.) and Grant-in-aid for Challenging Exploratory Research 20038784 from the Ministry of Education, Culture, Sports, Science and Technology. Japan (to N. F.).
The atomic coordinates and structure factors (codes 3W6Q and 3W6W) have been deposited in the Protein Data Bank (http://wwpdb.org/).
[1] To whom correspondence may be addressed. Tel.: 81-6-6879-8604; Fax: 81-6-6879-8606; E-mail: gkurisu@protein.osaka-u.ac.jp.
[2] To whom correspondence may be addressed. Tel.: 81-6-6879-7932; Fax: 81-6-6879-7935; E-mail: shinobu@mls.eng.osaka-u.ac.jp.

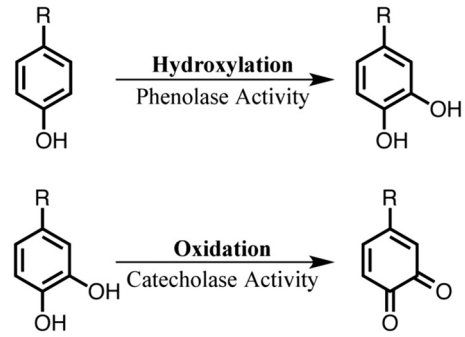

SCHEME 1

porter proteins, which transport copper from the extracellular medium to the cytoplasm (15). Therefore, the amount of free copper ions available in the cytoplasm of the cell is very limited. To survive under such copper-depleted conditions, copper chaperones are often employed to deliver copper ions into the active site of copper proteins. In this case, copper ions are accommodated by using multiple cysteine and/or methionine units from the conserved motifs CX_nC (n = 1–3) and/or MX_mM (m = 1, 2), which are crucial for copper chaperone activity in the proteins (15, 16).

For mammalian and yeast tyrosinases, it is thought that copper ions are transferred into the active site by Atox1 copper chaperone and copper-transporting ATPase (ATP7A), which catalyze copper movement across the membranes in the Golgi apparatus on the secretion process (15, 17). However, detailed mechanism of the copper incorporation process has yet to be elucidated. Recently, a copper chaperone, the so-called caddie protein (ORF378), was crystallized in the complex with the bacterial tyrosinase from *Streptomyces castaneoglobisporus* (9, 18), where ORF378 binds to the active site of tyrosinase to help the copper trafficking. This result provides some insights into the molecular mechanism of the copper incorporation process of type 3 copper proteins.

In the case of octopus hemocyanin, however, the dinuclear copper site is completely covered by an additional shielding domain (C-terminal domain) (7), thus prohibiting the direct access of a copper chaperone to the active site. The situation may be similar with fungal tyrosinase and plant catechol oxidase, which also involve a C-terminal shielding domain as mentioned below. In these cases, copper chaperone-like machinery may be equipped in the same protein to facilitate the copper incorporation. This has been proved in this study using fungal tyrosinase from *Aspergillus oryzae.*

With regard to the C-terminal domain, it may play an important role in regulating the enzyme activity. Namely, the C-terminal domain prohibits substrate access to the enzyme-active site and blocks the oxidase/oxygenase activity to avoid undesirable intracellular reactions of highly reactive quinonoid products. In support of this notion, several lines of evidence have indicated that a proteolytic enzyme *in vivo* cleaves a part of the protein of the fungal pro-tyrosinase and plant pro-catechol oxidase to induce the enzymatic activity (19–21). Furthermore, the cloned cDNA clearly indicates the existence of such an additional extension in the C-terminal domain, although the isolated active forms of mushroom tyrosinase (PPO3)[3] (12) and sweet potato catechol oxidase (8) lack the C-terminal domains in the crystal structures. On the basis of these results, it has been suggested that C-terminal domain of pro-tyrosinase is cleaved off by a proteolytic enzyme to produce the active form (Fig. 2, *B* to *C*) after copper ions are transferred into the active site through the protein shell (Fig. 2, *A* to *B*). However, the structural information of pro-tyrosinase has yet to be available, so that little is known about the details of the maturation processes, including the copper incorporation and the proteolytic activation.

We have recently reported that the apo-form of recombinant pro-tyrosinase from *A. oryzae* (inactive precursor) can be overproduced from *Escherichia coli* by using the full-length of *c*DNA (*melB*; 27% identity to the full-length sequence of PPO3), and reconstitution of this apo-pro-tyrosinase with copper ion under aerobic conditions induces autocatalytic formation of His^{94}–Cys^{92} cross-linkage in the enzyme-active site (22). The holo-pro-tyrosinase thus formed has no catalytic activity, but the trypsin treatment converts the holo-pro-form into the active form of the enzyme, in which the C-terminal domain (Gly^{464}–Ala^{616}) is absent (cleaved) (23).

Here, we successfully determined the crystal structures of the holo-pro- and the apo-pro-forms of *melB* tyrosinase from *A. oryzae* at a 1.39- and a 2.05-Å resolution, respectively, to provide the first detailed structural information about the fungal tyrosinase containing the C-terminal domain. The structural data of holo-pro-form provides important insights into the role of the C-terminal domain not only as a reactivity regulation domain but also as a copper chaperone-like machinery. Comparison of the crystal structures between the apo-pro-form and the holo-pro-form together with the mutagenesis studies have elucidated the detailed molecular mechanism of the maturation process of tyrosinase; the incorporation of copper ions and autocatalytic formation of the His-Cys cross linkage.

EXPERIMENTAL PROCEDURES

Expression of Tyrosinases and Selenomethionine-substituted Tyrosinase—melB pro-form of tyrosinase was prepared by using pETH-*melB* plasmid as described previously (22, 23). As for selenomethionine-substituted tyrosinase, expression plasmids were transformed into *E. coli* B834 (DE3) pLysS-competent cells. The transformants were grown in 2 liters of a baffled Erlenmeyer flask of 0.4 liters of Se-Met core medium (Wako) broth containing 50 mg/liter kanamycin, 4% glucose, 5 mg/liter vitamin B_1, 50 mg/liter L-SeMet, 1.2 g/liter $MgSO_4$, 24.4 mg/liter $FeCl_3$, 50 μl/liter 2 M HCl, 4% glucose, with shaking at 135 rpm at 25 °C until the cultures reached an A_{600} of 0.8. At this point, isopropyl 1-thio-β-D-galactopyranoside was added to the mixture (0.1 mM after addition), and the resulting mixture was allowed to continue being shaken for an additional 24 h at 18 °C.

Purification of Tyrosinase—If not mentioned otherwise, the same purification protocol was used for all proteins. *melB* pro-

[3] The abbreviations used are: PPO3, polyphenol oxidase 3; r.m.s.d., root mean square deviation; PDB, Protein Data Bank; BisTris, 2-[bis(2-hydroxyethyl) amino]-2-(hydroxymethyl)propane-1,3-diol; SeMet, selenomethionine; ICP-AES, inductively coupled plasma-atomic emission spectrometry.

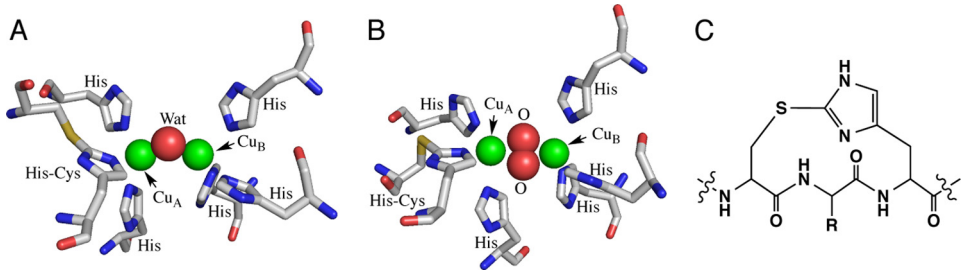

FIGURE 1. **Three-dimensional structures of the dinuclear copper sites containing a His-Cys cross-linkage.** *A*, potato catechol oxidase (PDB code 1BT1); *B*, octopus hemocyanin (PDB code 1JS8); *C*, ChemDraw structure of 2-cysteinyl-histidine (His-Cys) cross-linkage.

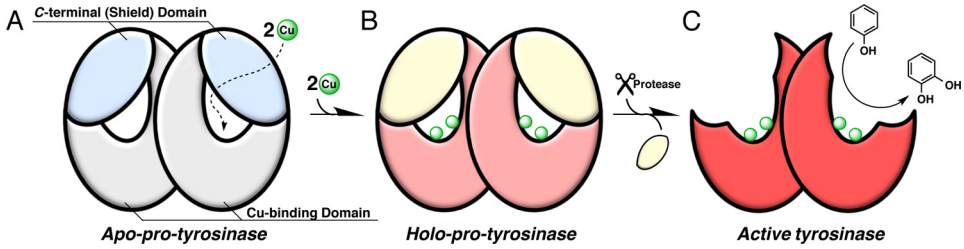

FIGURE 2. **Schematic representation of fungal tyrosinase maturation process.**

TABLE 1
Oligonucleotides used for site-directed mutagenesis

Name	Sequence (5′ →3′)[a]	Length	Use
MelBH332A-f1	GCGaactgggtgggaggattc	21	Forward primer for H332A
MelBH332A-r1	gacgttgttgtgaatagcttctaagttcatc	31	Reverse primer for H332A
MelBV359A-f1	ccagtggccgcgtatgatccgattttc	27	Forward primer for V359A
MelBV359A-r1	TGcactgctcatatggccagcaccccag	28	Reverse primer for V359A
MelBF513A-f1	agcggcagccttgaggacagtaactg	26	Forward primer for F513A
MelBF513A-r1	AGCgttgaagacactgcccacaaaattctg	30	Reverse primer for F513A
MelBC522A-f1	gacaagtgcgctcagcaagagcaag	25	Forward primer for C522A
MelBC522A-r1	TGCgttactgtcctcaaggctgccgctgaag	31	Reverse primer for C522A
MelBC525A-f1	gctcagcaagagcaagagggtgttttg	27	Forward primer for C525A
MelBC525A-r1	TGCcttgtcacagttactgtcctcaaggctg	31	Reverse primer for C525A
MelBC522A/C525A-f1	aagGCAgctcagcaagagcaag	22	Forward primer for C522A/C525A
MelBC522A/C525A-r1	gtcTGCgttactgtcctcaaggctgccgctgaag	34	Reverse primer for C522A/C525A

[a] The changed nucleotides are shown in capitals, and the codons corresponding to the amino acid residues to be changed are underlined.

tyrosinase was purified as described previously with some modifications (23). Harvested cells (~10 g) from 1 liter of culture were resuspended in 40 ml of the binding buffer (0.3 M NaCl, 10 mM imidazole, and 20 mM BisTris, pH 7.2) containing 0.2 mg/ml lysozyme. After 15 min of incubation on ice, the sample was sonicated 120 times for 5 s on ice (20-watt output). After centrifugation at 30,000 × *g* for 30 min, the clarified supernatant was loaded onto a 5-ml nickel-agarose column (COSMOGEL His-Accept, Nacalai Tesque) previously equilibrated with the binding buffer, and the histidine affinity tag-fused protein was eluted with nickel-Sepharose elution buffer (0.1 M imidazole, 0.3 M NaCl, 0.5 mM tris(2-carboxyethyl)phosphine, and 20 mM BisTris, pH 7.2). The histidine affinity tag-free pro-tyrosinase was released from the fusion protein by incubation with 2 units of HRV3C protease/mg of protein on ice for over 16 h. The protein solution was then dialyzed against 10 mM Tris-HCl buffer, pH 8.2, containing 10 mM imidazole at 4 °C to remove the excess imidazole and NaCl. The dialyzed solution was loaded onto a 5-ml nickel-agarose column previously equilibrated with this dialysis buffer again to remove the released histidine affinity-tagged protein. This eluent was subjected to anion-exchange chromatography by using a Q-Sepharose HP column (volume of 5 ml, GE Healthcare) with a linear gradient elution of NaCl (10–200 mM) in 10 mM Tris-HCl buffer, pH 8.2. The fractions containing pro-tyrosinase were collected and concentrated by ultrafiltration using a VIVA SPIN 20 (Sartorius). Before crystallization, the purified protein solution was desalted using a PD-10 column (GE Healthcare) and changed to 20 mM BisTris buffer, pH 7.2. The protein was stored at −80 °C until use. Purity was checked by SDS-PAGE.

Site-directed Mutagenesis—Oligonucleotide-directed mutagenesis experiments were performed on pETH-*melB* vector that contained *melB* cDNA. The pair of about 25-base mutagenic oligonucleotide (Table 1) was obtained from Integrated DNA Technology. Site-directed mutagenesis was carried out by the inverse PCR and following DpnI digestion and self-ligation. For the mutant, the absence of undesired mutations on the *melB* gene was confirmed by DNA sequence analysis using a 3100 Genetic Analyzer (Applied Biosystems) after the construction of the vector.

Quantification of Protein and Copper Content—Protein concentration was determined by a modified Lowry method using a DC protein assay kit (Bio-Rad) according to the supplier's manual. Copper concentration was determined by an ICP-AES on an ICPS-8100 (Shimadzu). The calibration curve of copper ion was made by using a copper ion standard solution (10.0 ppm).

TABLE 2
Data collection and refinement statistics

	Holo-form (PDB code 3W6W)	Apo-form (PDB code 3W6Q)	Se-SAD
Data set			
X-ray source	BL44XU	BL44XU	BL44XU
Space group	$P2_1$	$P2_1$	$P2_1$
Unit cell	a = 52.31 Å, b = 118.09 Å, c = 84.21 Å, β = 97.40°	a = 56.97 Å, b = 108.75 Å, c = 231.24 Å, β = 93.83 °	a = 54.03 Å, b = 118.16 Å, c = 78.78 Å, β = 91.40 °
Wavelength	0.90000 Å	0.90000 Å	0.97892 Å
Resolution[a]	50.00 to 1.39 Å (1.42 to 1.39 Å)	50.00 to 2.05 Å (2.09 to 2.05 Å)	50.00 to 2.52 Å (2.56 to 2.52 Å)
No. of total/unique reflections	736,459/198,757	606,461/175,066	122,994/33,456
Redundancy	1.9	1.3	1.9
Completeness[a]	98.3% (96.7%)	97.7% (84.7%)	98.8% (99.5%)
R_{merge}[a]	5.6% (76.3%)	5.1% (10.8%)	4.7% (10.6%)
I/σ[a]	28.8 (1.9)	38.7 (13.3)	42.8 (23.5)
Refinement			
R_{work}/R_{free}	17.74%/19.92%	14.39%/18.29%	
No. of protein/solvent atoms	9815/1095	18531/1820	
No. of metal ion atoms	4 (copper)	0	
B-factors of protein/solvent	18.1/27.9	24.1/30.8	
B-factors of metal ions	16.5		
r.m.s.d. bond/angle	0.009 Å/1.102°	0.007 Å/1.004°	
Ramachandran favored/allowed	98.7/1.3%	98.6/1.4%	

[a] Values in parentheses are for the highest resolution shells.

Crystallization of Copper-bound Pro-tyrosinase (Holo-pro-tyrosinase)—The protein sample was concentrated to 6 mg/ml by ultrafiltration using a VIVA SPIN 20 and reserved at −80 °C. Crystals of holo-pro-tyrosinase were obtained by the hanging drop vapor diffusion method. Crystallization droplets were prepared by mixing the precipitant solution containing 18% polyethylene glycol 3350, 50 mM NH_4F (1 μl), and 6 mg/ml tyrosinase solution (2 μl). Crystals were obtained at 4 °C in 1 day and were soaked in the solution containing 25% polyethylene glycol 3350, 50 mM NH_4F, and 20 mM BisTris at pH 7.2, for cryo-protection.

Crystallization of Copper-depleted Pro-tyrosinase (Apo-pro-tyrosinase)—The protein sample was concentrated to 17 mg/ml by ultrafiltration using a VIVA SPIN 20 and reserved at −80 °C. Apo-pro-tyrosinase was crystallized at 4 °C in a similar condition as holo-pro-tyrosinase using the precipitant solution containing 20% polyethylene glycol 3350, 50 mM KCl (1 μl), and 17 mg/ml tyrosinase solution (2 μl). For cryo-protection, solution containing 22.5% polyethylene glycol 3350, 15% ethylene glycol, 50 mM KCl, 20 mM BisTris at pH 7.2 was used.

Crystallization of Selenomethionine-substituted Pro-tyrosinase—The protein sample was concentrated in a similar condition as holo-pro-tyrosinase and crystallized at 4 °C using the precipitant solution containing 20% polyethylene glycol 3350, 50 mM NH_4F (1 μl), and 6 mg/ml tyrosinase solution (2 μl). The same solution as holo-pro-tyrosinase crystals was used for cryo-protection.

X-ray Data Collection—All diffraction data were collected at 100 K on the BL44XU beamline at the SPring-8 synchrotron facility (Harima, Hyogo, Japan). Before flash cooling, crystals were directly soaked in a respective cryoprotectant solution for 20 min. X-ray diffraction images were collected using an MX225HE CCD detector (Rayonix, Evanston, IL) equipped with a Helix Technology cryo-system (Cryo Industries of America, Manchester, NH). All diffraction images were recorded on the CCD camera, and the data were processed and scaled with the HKL-2000 program package. The data collection statistics are summarized in Table 2.

Phasing and Initial Model Building—We attempted to carry out molecular replacement using MOLREP (24). Mushroom tyrosinase (PDB code 2Y9W) was selected for molecular replacement because of its 27% amino acid similarity to *melB* tyrosinase. However, we were unable to obtain good solutions for the molecular replacement calculations. We also attempted to obtain the phase information using a copper single-wavelength anomalous dispersion and multiple-wavelength anomalous dispersion methods, but we have failed. Finally, the structure of Se-Met pro-tyrosinase was solved by the single-wavelength anomalous dispersion method using Se-Met-substituted pro-tyrosinase. Initial phases were calculated with the program AutoSolve (figure-of-merit, 0.48), and the structure model was continuously built with the program Automodel in Phenix program package (25). The resulting model covered 935 residues of the two subunits in the asymmetric unit with 738 side chains assigned. The initial model thus obtained, of which the R-factors are 0.284 (work) and 0.339 (free), was used as search model for phasing of the holo-pro-tyrosinase crystal.

Structure Determination—The structure of holo-pro-tyrosinase was solved by the molecular replacement method using the model of Se-Met tyrosinase as the search model. Automatic model-building program Autobuild in Phenix program package (25) built the initial model. The structure model was manually rebuilt with the program COOT (26) followed by refinement calculations with the program Phenix.refine, including TLS optimization (27). This procedure was iterated until the model did not further improve. During the refinement, the copper-ligand distances and the distance of His^{94}–Cys^{92} cross-linkage were loosely restrained with the ReadySet program. For apo-pro-tyrosinase, the structure was solved by molecular replacement using the final model of holo-pro-tyrosinase (chain A) as a search model, and the refinement procedure was the same as the case of holo-pro-tyrosinase. In both structures, Ramachandran analysis with the Molprobity program (28) showed no outliers. Secondary structures were assigned by the DSSP program (29). The atomic coordinates and structure factors for *melB* holo-pro-tyrosinase and apo-pro-tyrosinase were

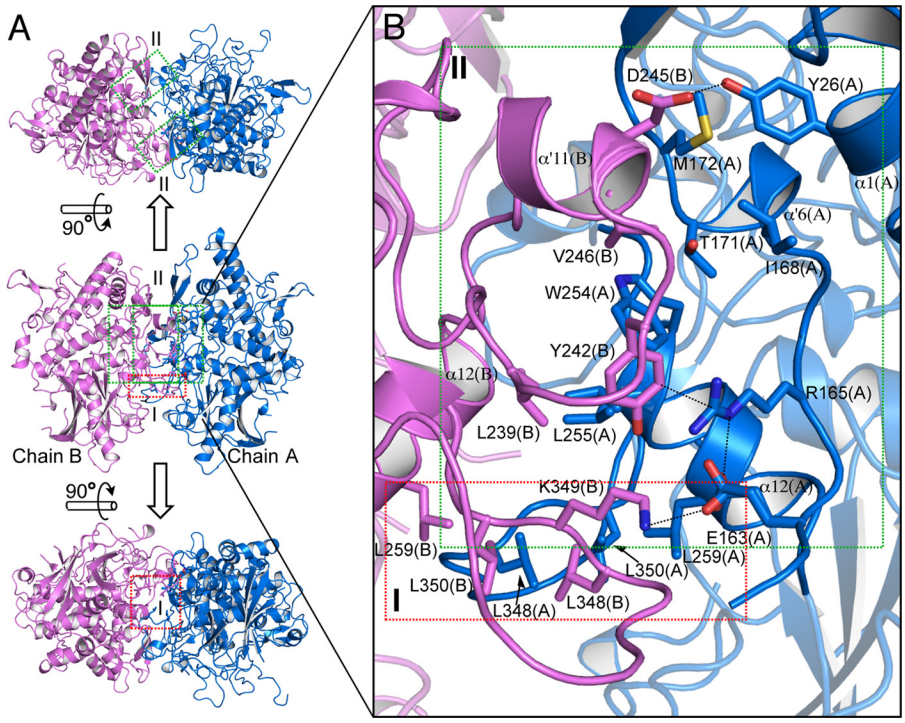

FIGURE 3. **Whole structure and dimer interfaces of *melB* holo-pro-tyrosinase.** *A,* homodimeric structure in the crystallographic asymmetric unit (*upper, top view*; *middle, side view*; *bottom, bottom view*). Subunit interfaces of the dimeric structure have three regions at the dimer interface, as indicated by *red* (*region I*) and *green* (*region II*) *rectangles*. Two same interactions of region II (*green*) exist in the interface (*upper*) along a 2-fold axis. The secondary structures are colored differently according to individual chains: chain A, *blue*; chain B, *pink*. *B,* magnified view of the two regions of dimer interface. Residues are shown as *sticks*. *Dotted lines* indicate closet contacts between atoms.

deposited in the PDB under the accession codes 3W6W and 3W6Q, respectively. All figures of protein structures were prepared using the program PyMOL (Version 1.3 Schrödinger, LLC).

Copper Uptake Assays—Copper binding assays were performed in *E. coli* BL21(DE3) cytoplasm. Expression of pro-tyrosinase was performed as reported previously (22, 23) except using the ZYM5052 medium (its copper concentration was determined to be <0.1 μM by ICP analysis) containing various concentrations of $CuSO_4$ (1 μM to 3 mM). Harvested cells were washed with 0.85% NaCl aqueous solution to remove the remaining copper ions on the cell surface at least three times. After the purification as described above without the step of anion-exchange chromatography, the copper content of pro-tyrosinase was determined by ICP-AES analysis. This experiment was performed at least two times for each mutant and copper concentration.

RESULTS AND DISCUSSION

Overall Structure of Holo-form of Full-length melB—The crystal structure of *melB* holo-pro-tyrosinase was determined by molecular replacement using the structure of the selenomethionine-substituted *melB* apo-pro-tyrosinase as a search model. Holo-pro-form was crystallized with one homodimer in the crystallographic asymmetric unit (space group $P2_1$). The final structures were refined to a resolution of 1.39 Å with excellent statistics (Table 2). Two protomers in the asymmetric unit are related by a noncrystallographic 2-fold axis (Fig. 3*A*), displaying an ellipsoid shape with dimensions of 95 × 65 × 45 Å (Fig. 3*A*). Elements of secondary structure (α for α-helix, α' for 3_{10}-helix, π for π-helix, and β for β-strand) are identified and numbered sequentially in Fig. 4.

The full-length *melB* protomer consists of 621 amino acid residues deduced from cDNA sequence. In chain B of the crystal structure, most of the residues were well defined in the final electron density, except for some disordered loops in the flexible regions (Gln^{81}–Pro^{88}, Asn^{158}–Gln^{160}, Ser^{213}–Ser^{222}, Asp^{304}–Gln^{316}, Gly^{515}–Gly^{532}, and Asp^{589}–Asp^{597}, Table 3). Conversely, the electron densities of three loops (Gln^{81}–Pro^{88}, Ser^{213}–Ser^{222}, and Gly^{515}–Gln^{527}) were observed in chain A. On the last loop, the backbone nitrogen atoms of Asp^{523}(A), Lys^{524}(A), and Cys^{525}(A) of chain A were hydrogen bonded to Asp^{552}(B′) and Asn^{492}(B′) of the next protomer (chain B′), the chain B molecule related by the crystallographic symmetry, respectively (Fig. 5). In addition, there is also a hydrogen bond between Asp^{523}(A) and Asp^{552}(B′). These results indicate that these hydrogen bonds fix one of the conformations of this loop (Gly^{515}–Gln^{527}) and further stabilized those of other two loops located in the neighbors (Gln^{81}–Pro^{88} and Ser^{213}–Ser^{222}).

Dimer Interface—melB pro-tyrosinase was found to exist mainly as a homodimer at physiological condition in our previous study (23). A very tight inter-protomer interaction was observed in the crystal structure of holo-pro-tyrosinase. The homodimer is glued together through extensive hydrophobic and charge-charge interactions, and the accessible surface area buried in the interface is 1925 Å^2 (Fig. 3*A*). Thus, we propose that the structure obtained via tight association is a biologically functional dimer. The dimer of holo-pro-tyrosinase is formed between chains A and B in a side-to-side manner along a 2-fold

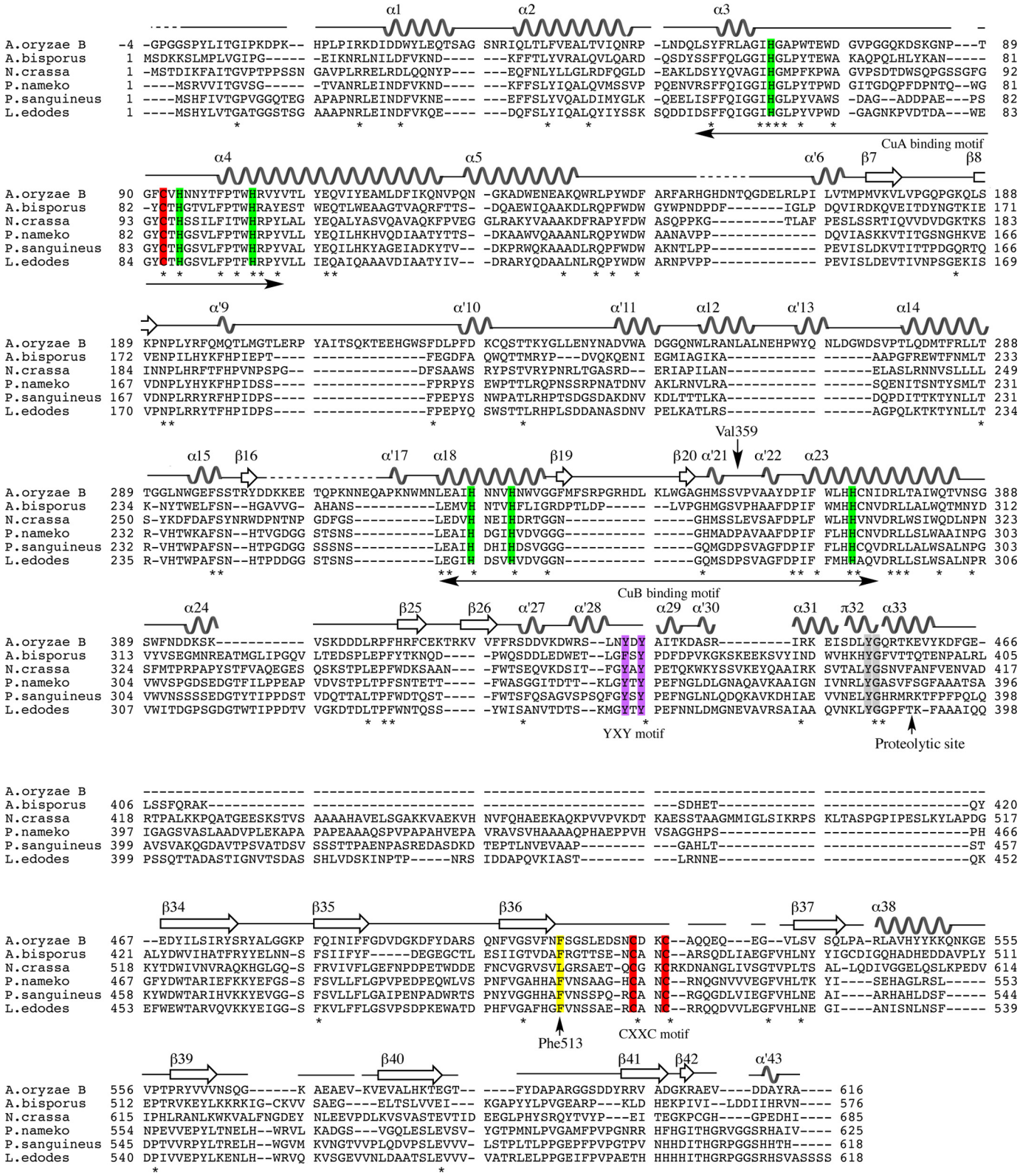

FIGURE 4. **Multiple sequence alignment of amino acid sequences of fungal tyrosinase and secondary elements of *melB* (α for α-helix, α′ for 3_{10}-helix, π for π-helix, and β for β-strand).** The alignment was generated with ClustalW by using MEGA5 software. The conserved residues are marked with an *asterisk* and *highlighted in rectangles* (*green*, copper-coordinating histidines; *red,* conserved cysteines; *yellow*, the place holder; *purple*, YXY motif; *gray*, YG motif). The *dashed line* indicates residues not visible in the electron density. *A. oryzae* B, *melB* from *A. oryzae* (BD165761); *A. bisporus*, PPO3 from *Agaricus bisporus* (CAA59432); *N. crassa*, *Neurospora crassa* (CAE81941); *P. nameko*, *Philiota nameko* (AB275647); *P. sanguineus*, *Pycnoporus sanguineus* (AAX46018); *L. edodes*, *Lentinula edodes* (BAB71735).

TABLE 3
Missing residues and atoms

Holo-form				
Missing residues				
Chain A	Gly (−4)-Gly (−2)	His^{154}–Gln^{160}	Lys^{305}–Ala^{316}	Asp^{589}–Asp^{597}
Chain B	$Gly^{(-4)}$–$Gly^{(-1)}$	Gln^{81}–Pro^{88}	Asn^{158}–Gln^{160}	Ser^{213}–Ser^{222}
	Asp^{304}–Gln^{316}	Gly^{515}–Gly^{532}	Asp^{589}–Asp^{597}	
Missing atoms				
Chain A	Lys^{215} (Cϵ, Nζ)	Lys^{395} (Cϵ, Nζ)	Lys^{413} (Cδ, Cϵ, Nζ)	
	Lys^{524} (Cδ, Cϵ, Nζ)	Lys^{606} (Cϵ, Nζ)		
Chain B	Lys^{123} (Cϵ, Nζ)	Phe^{223} (Cγ, Cδ1, Cδ2, Cϵ1, Cϵ2, Cζ)		
	Lys^{319} (Cγ, Cδ, Cϵ, Nζ)	Lys^{397} (Nζ)	Lys^{413} (Cδ, Cϵ, Nζ)	
	Asp^{440} (Cγ, Oδ1, Oδ2)	Lys^{482} (Cϵ, Nζ)		
Apo-form				
Missing residues				
Chain A	Lys^{82}–Lys^{85}	Gly^{155}–Gln^{160}	Ser^{213}–Phe^{223}	Asp304--Gln^{316}
	Ser^{516}–Gly^{532}	Arg^{593}–Asp^{597}		
Chain B	$Gly^{(-4)}$–$Gly^{(-1)}$	Gln^{81}–Gly^{86}	Gly^{155}–His^{156}	Ser^{213}–Phe^{223}
	Asp^{304}–Gln^{316}	Ser^{516}–Gly^{532}	Pro^{591}–Asp^{597}	
Chain C	$Gly^{(-4)}$–$Gly^{(-1)}$	Lys^{82}–Gly^{86}	Gly^{155}–Gln^{160}	Ser^{213}–Ser^{222}
	Asp^{304}–Asp^{316}	Ser^{516}–Gly^{532}	Pro^{591}–Gly^{595}	
Chain D	Gln^{81}–Asn^{87}	Gly^{155}–Asn^{158}	Ser^{213}–Ser^{222}	Asp^{304}–Gln^{316}
	Ser^{516}–Gln^{531}	Pro^{591}–Asp^{597}		
Missing atoms				
Chain A	Lys^{13} (Cϵ, Nζ)	Lys^{123} (Cδ, Cϵ, Nζ)	His^{154} (Cγ, Nδ1, Cδ2, Cϵ1, Cϵ2)	
	Lys^{395} (Cϵ, Nζ)	Lys^{413} (Cϵ, Nζ)		
Chain B	Lys^{13} (Cϵ, Nζ)	Lys^{319} (Cϵ, Nζ)	Arg^{345} (Cδ, Nϵ, Cζ, Nη1, Nη2)	
	Lys^{397} (Cδ, Cϵ, Nζ)	Lys^{413} (Cϵ, Nζ)	Asp^{440} (Cγ, Oδ1, Oδ2)	
	Lys^{606} (Cϵ, Nζ)			
Chain C	His^{154} (Cγ, Nδ1, Cδ2, Cϵ1, Cϵ2)	Lys^{395} (Cϵ, Nζ)	Lys^{397} (Cδ, Cϵ, Nζ)	
	Arg^{443} (Cδ, Nϵ, Cζ, Nη1, Nη2)	Lys^{553} (Cδ, Cϵ, Nζ)	Ser^{596} (Cγ)	
	Arg^{601} (Nη1, Nη2)	Glu^{609} (Cδ,Oϵ1, Oϵ2)		
Chain D	Lys^{13} (Cϵ, Nζ)	Lys^{123} (Cδ, Cϵ, Nζ)	Lys^{395} (Cϵ, Nζ)	
	Glu^{531} (Cγ, Cδ, Oϵ1, Oϵ2)	Lys^{553} (Cϵ, Nζ)		

axis; thus, the substrate-binding pockets face alternate directions so as not to interfere with each other. The dimer interface can be classified into three regions (Fig. 3*A*, indicated by *green* and *red rectangles*). Region I (*red region*) predominantly involves hydrophobic interactions among leucine clusters (Leu^{259}(A), Leu^{348}(A), Leu^{350}(A), Leu^{259}(B), Leu^{348}(B), and Leu^{350}(B), Fig. 3*B*, *red*). The interface of region II (Fig. 3*B*, *green region*) is stabilized by hydrogen bonds between Tyr^{26}(A) and Asp^{245}(B), salt bridge between Glu^{163}(A) and Lys^{349}(B), and cation-π interaction between Arg^{165}(A) and Tyr^{242}(B). Furthermore, a tight hydrophobic interaction through van der Waals contacts is situated at the heart of region II (Thr^{171}(A), Trp^{254}(A), Leu^{255}(A), Leu^{239}, Tyr^{242}(B), and Val^{246}(B), Fig. 3*B*, *green*). Thus, both polar and hydrophobic interactions stabilize the association of the A and B chains.

Domain Structure of Holo-form of Full-length melB from A. oryzae—Each protomer consists of two structural domains as follows: the N-terminal copper-binding domain (Ser^{1}–Phe^{463}, indicated by *blue*) and the C-terminal shielding domain (Gly^{464}–Ala^{616}, indicated by *red*) (Fig. 6*A*). Because two protomers are nearly identical to each other, we describe the monomer structure by referring mainly to the chain-A molecule. The copper-binding domain includes the central core structure (Arg^{19}–Tyr^{435}) (3) and the peripheral loop region connecting the secondary structure elements (Figs. 4 and 6*C*). While *melB* pro-tyrosinase having about 100 extra residues is much larger than mushroom tyrosinase (PPO3, PDB code 2Y9W), the core structure was almost identical to that of the mushroom tyrosinase (root mean square deviation (r.m.s.d.) value for Cα atoms of 351 matched residues is 2.5 Å, Figs. 4 and 6*C*). A significant structural difference has arisen between the loop regions surrounding the core structures (Fig. 6*C*). The *melB* core structure is also similar to those of the other type 3 copper proteins, sweet potato catechol oxidase (PDB code 1BT3, r.m.s.d. 3.3 Å, 261 matched residues) and the functional unit of octopus hemocyanin (PDB code 1JS8, r.m.s.d. 2.9 Å, 258 matched residues) (Fig. 6, *E* and *F*). In these proteins, including *melB* tyrosinase, a four-helix bundle of the core structure provides the highly conserved six histidine residues as the copper ligands (three histidine imidazoles for each copper ion, Cu_A and Cu_B) in the active site, and one of these histidines (His^{94}, *melB* numbering) is covalently bound to nearby cysteine (Cys^{92}, *melB* numbering) via a thioether linkage (Fig. 6, *B*, *D,* and *F*).

The dinuclear copper center of *melB* tyrosinase is buried in the cleft of the copper-binding domain and is inaccessible to the exterior solvent due to the occlusion by the C-terminal domain as expected. The tip of the C-terminal domain is the Phe^{513} residue, and its side chain is accommodated just above this dicopper active center as the "placeholder" for phenolic substrates (Fig. 6*B*). The phenyl ring of Phe^{513} stacks onto the imidazole ring of one of the Cu_B ligands (His^{332}) at the distance of ~3.6 Å, and the edge of the aromatic ring is close to Cu_B (~3.9 Å, Fig. 6*B*). Furthermore, one conformer of the side chain of Val^{359} residue (Val^{359}(A)) is also at a van der Waals distance (~3.5 Å) from the aromatic ring of Phe^{513} residues (Fig. 6*B*). Notably, the mutant V359A could be expressed in the soluble fraction in *E. coli*, whereas mutants H332A and F513A were expressed as inclusion body (Fig. 7), indicating that the π-stacking between Phe^{513} and His^{332} may strongly contribute to the stabilization of inter-domain interaction in *melB* pro-tyrosinase (Fig. 6, *A* and *B*).

The C-terminal domain exhibits a seven-stranded antiparallel β-sandwich structure, whose topology is the truncated jelly-roll motif (Fig. 8, *A* and *D*). The C-terminal domain does not

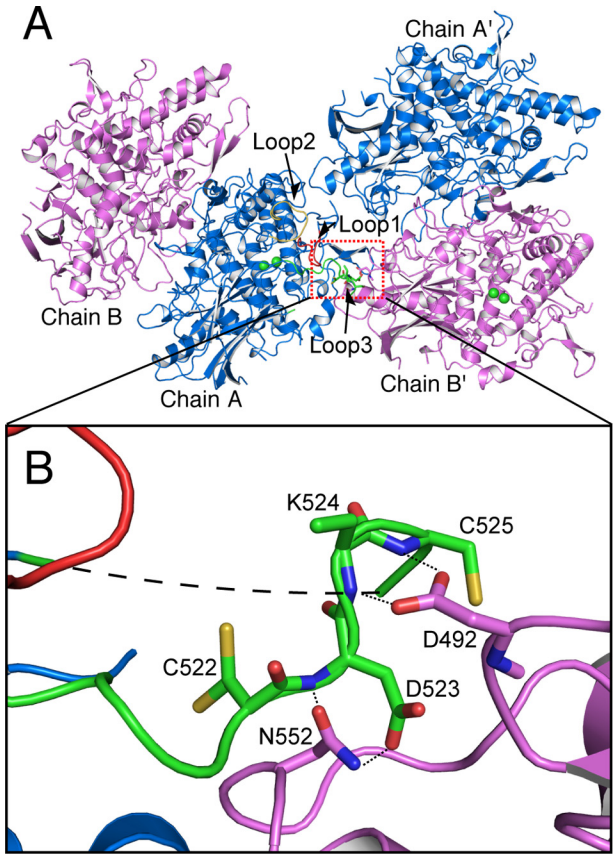

FIGURE 5. **Interaction between the flexible loop and the next protomer related by the crystallographic symmetry.** *A,* two homodimeric structures of holo-pro-form related by the crystallographic symmetry. Colored loops are loop 1 (Lys^{82}–Lys*85*, *red*), loop 2 (Ser^{213}–Phe^{223}, *yellow*), and loop 3 (Ser^{516}–Gly^{532}, *green*) of holo-pro-form chain A. *B,* magnified view on the contacting region indicated by *dotted rectangle*. *Dotted lines* and *small dashed line* indicate the closet contacts between atoms, and the long *dashed line* indicates residues not visible in the electron density.

show any structural similarity to the caddie protein of *S. castaneoglobisporus* tyrosinase (Fig. 8*C*). By structural similarity search using the DALI server (30), the closest structural homolog was found in the shielding domain of octopus hemocyanin functional unit (Fig. 8*B,* PDB code 1JS8, r.m.s.d. 2.5 Å, 89 matched residues) despite little sequence identity (7%), the copper-binding domain of which is also structurally similar to that of *melB* tyrosinase described above. Thus, the protomer can be superimposed to that of octopus hemocyanin not only with the copper-binding domain but also with the C-terminal domain (Fig. 6*E*). Consistent with the structural similarity, the holo-pro-tyrosinase has no catalytic activity, but the reduced form of holo-pro-tyrosinase produced by the reduction of the as-isolated enzyme with hydroxylamine exhibits a reversible dioxygen-binding ability, and its affinity toward dioxygen is almost equal to that of octopus hemocyanin (23). The Leu^{2830} residue in the octopus hemocyanin structure occupied a similar position as Phe^{513} in *melB* tyrosinase (Fig. 6*F*), so the aromatic carbons of Phe^{513} might not have much influence on the dioxygen-binding ability.

The proteolytic digestion of the C-terminal domain having Phe^{513} placeholder leads to opening the entrance to the enzyme-active site for substrate incorporation (Fig. 2, *B* to *C*). In the copper-binding domain, the core region (Arg^{19}–Tyr^{435}) is followed by a linker consisting of 28 residues (Ala^{436}–Lys^{463}), which contains the five short helices (α29, α'30, α31, π32, and α33, see Figs. 4 and 9). This linker region has an inflection point containing conserved Tyr-Gly sequence motif (Tyr^{452} and Gly^{453}), located in the π-helix (π32, Fig. 9). In the proteolytic activation in our previous study, the C-terminal domain and the last part of this linker (α33) were digested (Glu^{458}–Ala^{616}, see below) (23). The hydroxyl group of Tyr^{452} has hydrogen bonds to the side chains of the functionally conserved Asp^{147} and Arg^{377}, enforcing this region of the linker to associate with the tyrosinase core domain (Fig. 9). Thus, this linker moiety is situated on the surface of the monomer, and the α33 helix is bulged out from the surface of the copper-binding domain, so the proteolytic enzyme can easily attack this region. This cleavage site (between Lys^{457} and Glu^{458}) is also located next to the equivalent C-terminal position in the active mushroom tyrosinase (PPO3).

Conserved Cysteines in melB Apo-pro-tyrosinase—As in the case of holo-pro-tyrosinase, *melB* apo-pro-tyrosinase exhibits a homodimeric structure. The crystal structure of apo-pro-form of *melB* was determined by molecular replacement using the structure of holo-pro-form as a search model. The final structure of apo-pro-form was refined to a resolution of 2.05 Å with good statistics (Table 2). Apo-pro-form *melB* tyrosinase was crystallized in the monoclinic space group of $P2_1$. Most of the residues are well defined in the final model in each protomer (Fig. 10*A*), and the crystallographic asymmetric unit has two sets of homodimers (chains A and B and chains C and D). Four protomer molecules are almost identical to each other and very similar to those of the holo-pro-form (Fig. 10*B*). In chain A, the six disordered loops and peptide side chains were observed (Lys^{82}–Lys^{85}, Gly^{155}–Gln^{160}, Ser^{213}–Phe^{223}, Asp^{304}–Gln^{316}, Ser^{516}–Gly^{532}, and Arg^{593}–Asp^{597}), as is the case of chain B of holo-pro-form structure. The whole structures of apo-pro-form and holo-pro-form closely resemble each other, showing a 0.5-Å r.m.s.d. over all backbone atoms except the disordered region (chain A and B of apo-pro-form crystal *versus* chain A and B of holo-pro-form crystal).

Despite the similarity of the whole structures, the positions of the three-conserved histidine residues (His^{94}, His^{332}, and His^{372}) of apo-pro-form are different from those of the holo-pro-tyrosinase, and a water molecule (Wat^{701}) is present in place of the two copper ions (Figs. 10*C* and 11, *A* and *B*). Wat^{701} is hydrogen-bonded to three Nϵ2 nitrogen atoms of the imidazole groups of His^{67}, His^{94}, and His^{103} (<3.0 Å Cu_A-coordinating), but those of the other histidines (>3.0 Å Cu_B-coordinating) are not within hydrogen-bonding distance. The side chains of His^{94} and His^{372} take different conformations from those of the holo-pro-form and exhibited higher average *B*-factors (33.3 and 19.5 Å^2, respectively) than those of the other four histidines (14.3 Å^2). These results suggest that the side chain of these two histidine residues are flexible as compared with those of the others; His^{94} and His^{372} imidazoles exhibit no hydrogen-bonding interaction with other protein residues. The positions of side chains His^{332} and Phe^{513} deviate somewhat from those in holo-pro-tyrosinase due to the absence of the metal coordination (Fig. 11*D*). It should be noted that no electron density

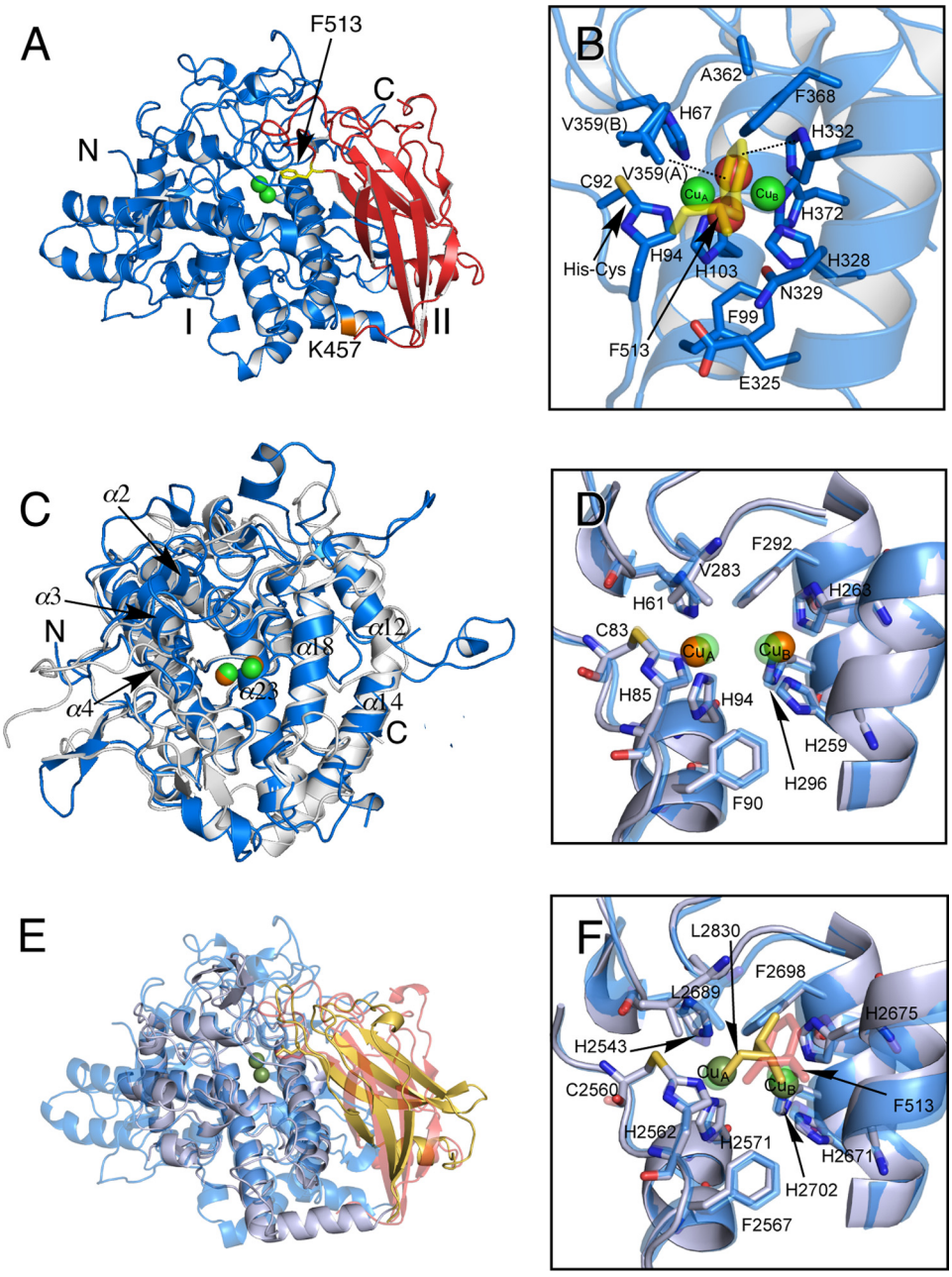

FIGURE 6. **Crystal structure of protomer of *melB* holo-pro-tyrosinase.** *A,* structure of the chain A molecule. The copper-binding domain (domain I, Ser^{1}–Phe^{463}) is colored in *blue* and the C-terminal domain (domain II, Gly^{464}–Ala^{616}) in *red*. Putative proteolytic site (Lys^{457}) is labeled and shown in *orange*. The N and C termini are indicated as *N* and *C*, respectively. The *black arrow* indicates Phe^{513} from the C-terminal domain covering the active site. *B,* active site structure viewed from the C-terminal domain. Phe^{513} is shown as a *stick model* colored in *yellow*. *Dotted lines* indicate closest contacts between atoms. *C,* superimposed structure of the copper-binding domain (*blue*) *versus* mushroom tyrosinase (PDB code 2Y9W) (*gray*). *D,* superimposed structure of active site structure of *melB* (*cyan*) *versus mushroom* tyrosinase (PDB code 2Y9W) (*gray*). *E,* superimposed structure of whole structure of *melB* (the copper-binding domain in *cyan*, and the C-terminal domain in *red*) *versus Octopus* hemocyanin (PDB code 1JS8) (*gray* and *yellow*). *F,* superimposed structure of active site structure of *melB* (*cyan*) *versus Octopus* hemocyanin (PDB code 1JS8) (*gray*). Both *green* and *brown spheres* and *red spheres* indicate copper and water, respectively. Residues are shown as *sticks*.

was found between Cys^{92} and His^{94} side chains (Fig. 11*B*), definitely demonstrating that the His^{94}–Cys^{92} thioether linkage is absent in the apo-form, and the covalent His-Cys bond is formed after the copper up-take as reported in our previous paper (22). Furthermore, the side chain of Cys^{92} adopts dual conformations: one (Cys^{92}(A)) is exactly the same as the conformation observed in the holo-form and the other one (Cys^{92}(B)) faces to the direction to the Cu_A-binding site (Figs. 10*C* and 11*B*). In the latter conformation, S atom of Cys^{92} side chain is within bonding distance to Cu_A (< 2.5 Å), suggesting a direct interaction of the thiol (or thiolate) group of Cys^{92} and copper ion(s) during the maturation process.

It should be noted that the electron density of the surface region enveloping the Cu_A-binding site is completely disordered in each protomer of apo-pro-tyrosinase. This area is composed of three loops (loops 1–3: Lys^{82}–Lys^{85}, Ser^{213}–Phe^{223}, and Ser^{516}–Gly^{532}, see Figs. 10*B* and 11*C*). From the amino acid sequence analysis of these flexible loops, a C*XX*C

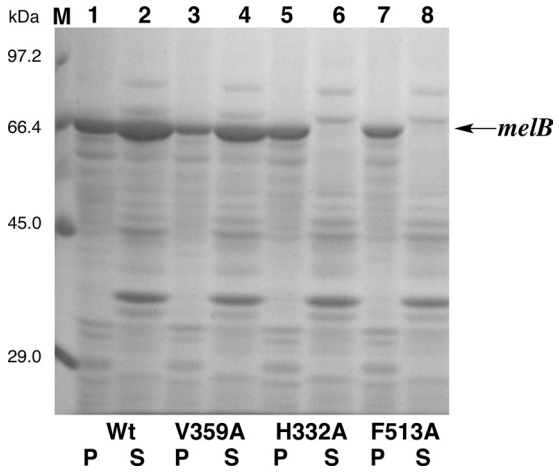

FIGURE 7. **SDS-12.5% PAGE.** Precipitation (*P*) (*lanes 1, 3, 5,* and *7*) and supernatant (*S*) (*lanes 2, 4, 6,* and *8*) of cell extract of *E. coli* containing *melB* expression plasmid. *Lane M,* marker; *lanes 1* and *2*, wild type; *lanes 3* and *4*, V359A; *lanes 5* and *6*, H332A; *lanes 7* and *8*, F513A. *Arrows* indicates the bands of *melB* pro-tyrosinase.

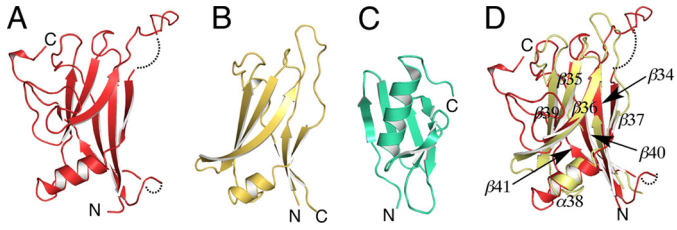

FIGURE 8. **Structure of C-terminal domains and caddie protein.** *A,* structure of the C-terminal domain of *melB* holo-pro-tyrosinase. *B,* structure of the shielding domain of the functional unit of *Octopus* hemocyanin (PDB code 1JS8). *C,* structure of the caddie protein of *S. castaneoglobisporus* tyrosinase (PDB code 1WX2). *D,* superimposed structure of the C-terminal domain of *melB* (*red*) *versus* shielding domain of octopus hemocyanin (PDB code 1JS8) (*yellow*). The *dotted line* indicates the residues not visible in the electron density.

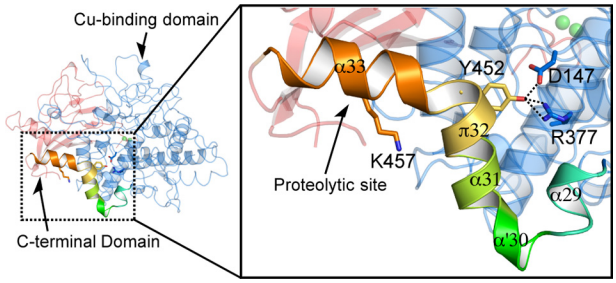

FIGURE 9. **Structure of the linker region between the core and C-terminal domains.** Location of the proteolytic site in the molecule. Magnified view of the C-terminal region of the copper-binding domain shows the interactions between YG motif and core region. *Dashed lines* show hydrogen bonds.

motif composed of the conserved two cysteines (Cys^{522} and Cys^{525}, Figs. 4, 10*B*, and 11*C*) are found on loop 3 of the C-terminal domain. Such a motif is seen in the copper chaperones such as Atox1 and Ccc2 in yeast (15). Thus, we consider that the three cysteines (Cys^{92}, Cys^{522}, and Cys^{525}) are involved in the copper uptake process (Fig. 2, *A* to *B*).

Assembling Process of Dinuclear Copper Center—To confirm this hypothesis, we have performed a copper uptake experiment from the *E. coli* cytoplasm by using Cys-to-Ala mutants. The extent of assembly of the dinuclear copper center of as-isolated *melB* pro-tyrosinase practically depended on the $CuSO_4$ concentration in the medium (Fig. 12, *black circles*). From this

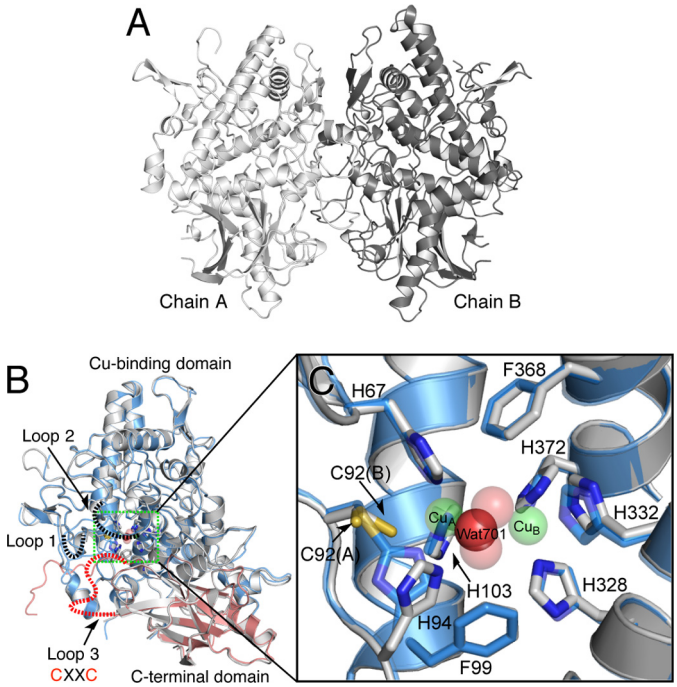

FIGURE 10. **Crystal structure of *melB* apo-pro-tyrosinase.** *A,* homodimeric structure of the apo-pro-form (*gray* and *dark gray*). *B,* subunit structures of apo-pro-form (chain A, *gray*) *versus* holo-pro-form (chain A, *cyan*, copper-binding domain; *red,* C-terminal domain). *Dotted lines* indicate the disordered loops colored in *black* and *red*. *C,* magnified view on the active site region of apo-pro-form (chain A, *gray*) and holo-pro-form (chain A, *transparent cyan* and *sphere*) indicated by the *green rectangle*. *Green* and *red spheres* indicate copper and water, respectively. Residues are shown as *sticks* and colored by atom type (carbon, as the respective structural element; nitrogen, *blue*; oxygen, *red*).

result, it was thought that the influx of the copper(II) ion into the *E. coli* cytoplasm might increase as the $CuSO_4$ concentration in the medium becomes higher. The redox state of the copper becomes a monovalent cation (copper(I)) in the cytoplasm of *E. coli* as in the eukaryotic cells (31). Wild type of *melB* pro-tyrosinase was successfully metalated to full complement even at a low concentration of $CuSO_4$ (~1 mM). However, C522A and C525A mutants (Fig. 12, *blue* and *green circles*, respectively) needed more than 1 order of magnitude higher concentration of $CuSO_4$ in the medium to complete the assembly of the dinuclear copper center, and a full complement of double mutants (C522A/C525A, Fig. 12, *orange circle*) was not observed within the range of the concentration capable of growing *E. coli* (≤3 mM). Furthermore, C92A mutants (C92A and C92A/C522A/C525A, Fig. 12, *red* and *purple circle,* respectively) have almost no ability to incorporate the copper ions from the cytoplasm of *E. coli*. Thus, it could be concluded that Cys^{92} residue as well as the $^{522}CXXC^{525}$ motif contributes to the copper incorporation of *melB* apo-pro-tyrosinase (Fig. 2, *A* to *B*).

From these results, we concluded that the C-terminal shielding domain functions not only to control the enzyme activity by prohibiting the substrate access but also to induce the copper incorporation into the active site like copper chaperone. The completely disordered region of this shielding domain (loop 3) exists near Cu_A site and contains the two highly flexible cysteines (Cys^{522} and Cys^{525}) within the distance range of about

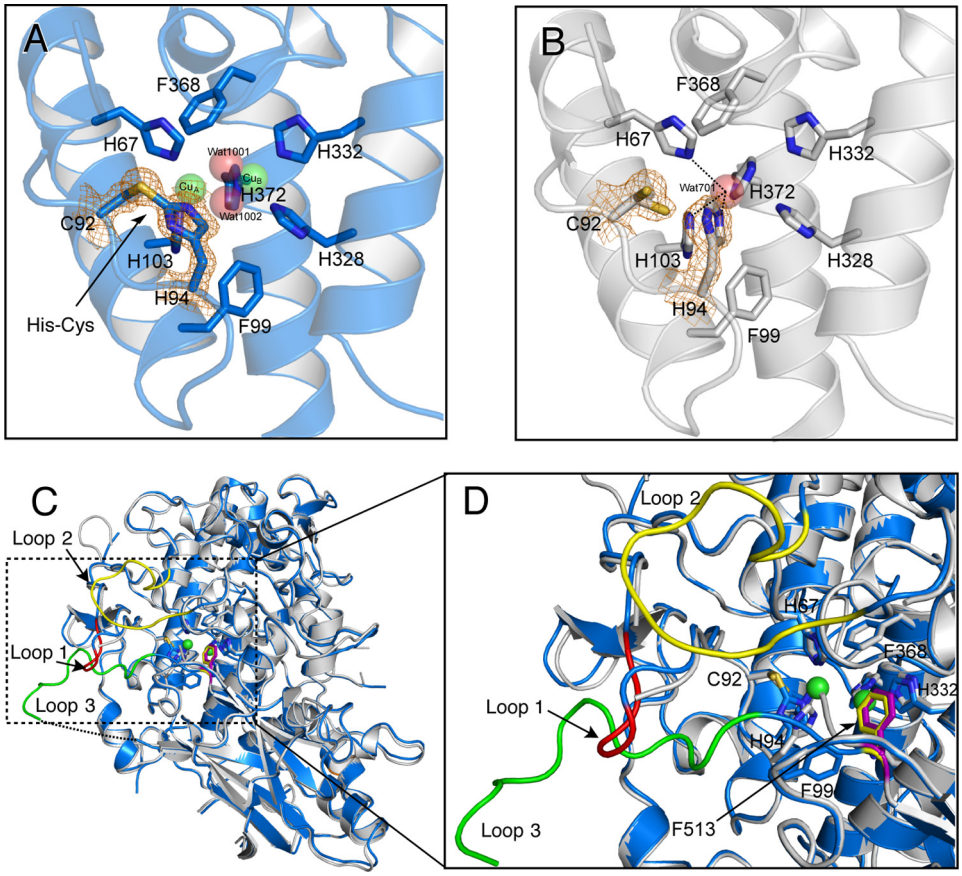

FIGURE 11. **Structural comparison of the holo-pro-form and apo-pro-form *of melB*.** *A*, His^{94}–Cys^{92} linkage of the holo-pro-form, and *B*, free Cys^{92} and His^{94} side chains of the apo-pro-form covered with electron density map (σ level = 1.5). *C*, superimposition of apo-form chain A (*gray*) and holo-form chain A (*blue*). *Dashed rectangle* indicates the disordered region of apo-pro-form chain A. Colored loops in this rectangle are loop 1 (Lys^{82}–Lys^{85}, *red*), loop 2 (Ser^{213}–Phe^{223}, *yellow*), and loop 3 (Ser^{516}–Gly^{532}, *green*) of holo-pro-form chain A. *Dotted lines* indicate the residues not visible in the electron density. *D*, superimposed structure of the active site region of apo-pro-form (chain A, *gray*) and holo-pro-form (chain A, *blue* and *sphere*). Residues are shown as *stick models*. *Dotted lines* indicate the closet contacts between atoms. Phe^{513} id shown as a stick model colored in *yellow* (holo) and *purple* (apo). *Green spheres* indicate copper ions.

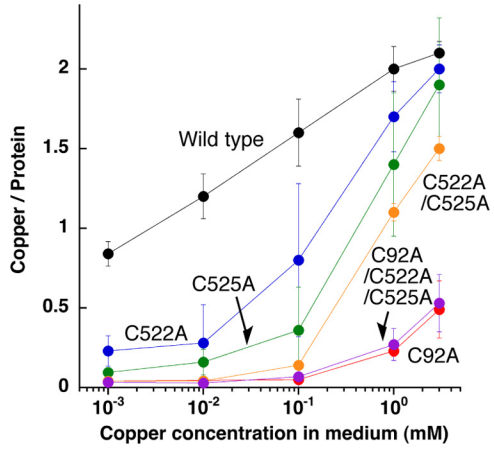

FIGURE 12. **Copper content *versus* $CuSO_4$ concentration.** Copper content of purified pro-tyrosinase from *E. coli* cultivated in the medium containing various concentrations of $CuSO_4$. Wild type, *black*; C92A, *red*; C522A, *blue*; C525A, *green*; C522A/C525A, *orange*; C92A/C522A/C525A, *purple*.

5–15 Å from the sulfur atom of Cys^{92}. This structural feature is reminiscent of the action of copper chaperones. The ^{522}*CXXC*^{525} motif may act as the linear bidentate ligand to copper(I) (Fig. 13*B*) and serve as a copper shuttle to Cys^{92}, where the copper(I) ion may be transiently ligated by three cysteine residues (Fig. 13, *B* to *C*). Another copper(I) ion may be incorporated in the similar manner to produce a dicopper(I) form of the reduced enzyme (Fig. 13, *D* to *E*). During this process, Cys^{92} may switch the conformation between Cys^{92}(A) and Cys^{92}(B), enhancing the copper(I) transport into a Cu_A binding site (Fig. 13, *C* to *E*). From the dicopper(I) species thus constructed (Fig. 13*E*), (μ-η^2/η^2-peroxido)dicopper(II) species is generated by the reaction with dioxygen (Fig. 13*F*). As demonstrated in our previous study, the His-Cys cross-linkage formation proceeds autocatalytically involving the formation of this active species as a key intermediate to produce the Met-pro-tyrosinase (dicopper(II), Fig. 13*G*) (22). As a result, two copper ions can be transported into the active site by the contribution of these cysteines (Cys^{92}, Cys^{522}, and Cys^{525}).

Maturation Process of melB Tyrosinase—In this study, we have obtained the detailed structural information of fungal pro-tyrosinase containing the shielding C-terminal domain, which covers the entrance of the active site. We have confirmed that three cysteines (Cys^{92}, Cys^{522}, and Cys^{525}) play significant roles in the copper incorporation process. Fungal tyrosinase exploits the thiol group of Cys^{92} for the metal incorporation as well as enhancement of the enzymatic activity as described in our previous paper (22). In this context, the His-Cys-forming cysteines found in octopus hemocyanin and sweet potato catechol oxidase may also participate in the copper incorporation process

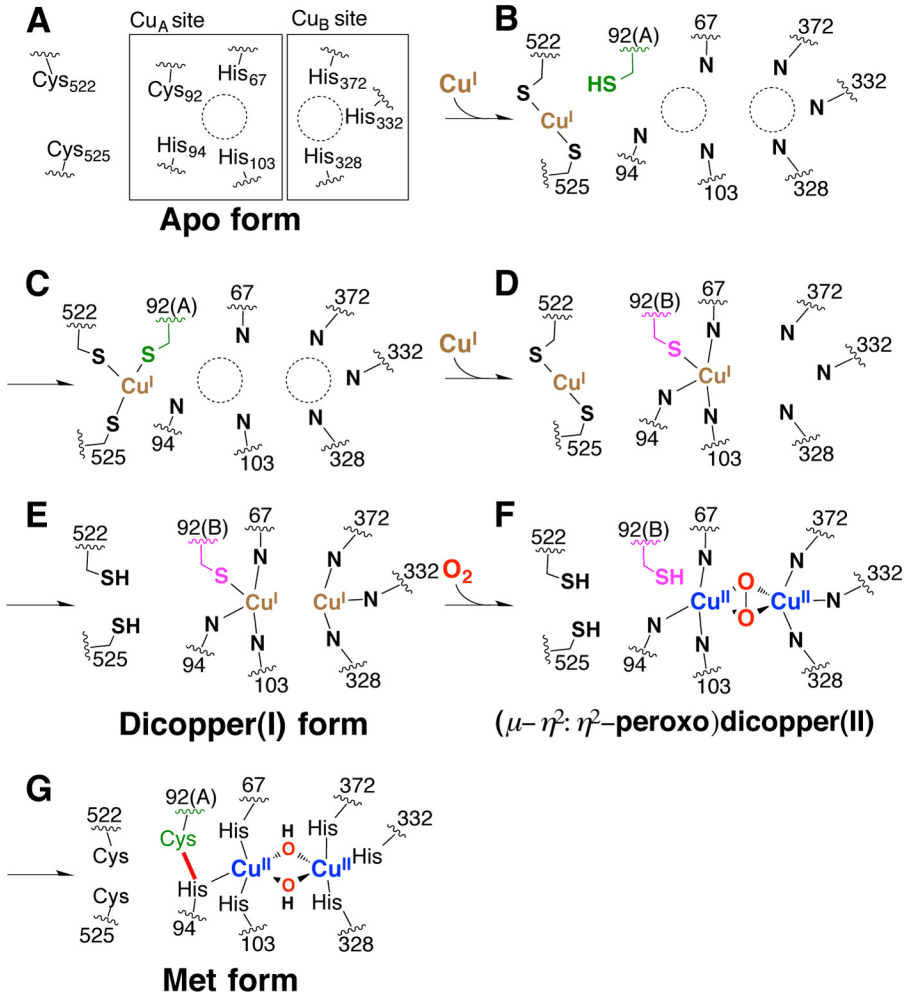

FIGURE 13. **Schematic representation of putative copper incorporation process into pro-tyrosinase.**

(Fig. 1, *A* and *B*). Although *CXXC* motifs like fungal tyrosinase are not conserved on the C-terminal domain of these proteins, we were able to find a disulfide bond in the proximity of their His-Cys cross-linkage (within 10 Å distance) on the copper-binding domain in each crystal structure (octopus hemocyanin, Cys^{2549}–Cys^{2559}, and sweet potato catechol oxidase, Cys^{27}–Cys^{89}), indicating that the free thiol form of these disulfides may have similar functions to that of $^{522}CXXC^{525}$ motif of *melB* tyrosinase. Besides Cys^{92}, two cysteines (Cys^{522} and Cys^{525}) on the C-terminal domain are highly conserved among any fungal tyrosinases (Fig. 4), whereas the specific partner protein for tyrosinase as a copper chaperone has not been found in the fungi yet. Therefore, the fungal tyrosinase may assemble the dinuclear copper center by itself by using the internal three cysteines, directly transferring from copper permeases on the cytoplasmic membrane such as Ctr1/3 homologs (15) without the mediation by the external copper chaperones (Fig. 2, *A* to *B*). However, the exact interaction between tyrosinase and such copper permeases is not known; therefore, the detailed molecular mechanism of the copper transfer between these proteins needs further investigation.

We have examined that the trypsin treatment induces the activation of *melB* holo-pro-tyrosinase and explored its activation mechanism (Fig. 2, *B* to *C*); the tryptic digestion induced cleavage of the C-terminal domain (Glu^{458}–Ala^{616}) while keeping the dimeric structure of the enzyme (23). As mentioned above, the interactions between subunits are located in the copper-binding domain predominantly, indicating that the dimeric structure is retained after cleavage of the C-terminal domain involving the activation process. The core structure of copper-binding domain is almost identical to that of the active form of mushroom tyrosinase (PPO3) as well as catechol oxidase. Therefore, we could conclude that this cleavage process induces little conformational change of the active site but simply causes the removal of Phe^{513} from the active site (Fig. 6, *A* and *C*). To our knowledge, no protease specific to tyrosinase has been discovered yet, but the proteases with trypsin-like activity are common in fungi (32). Thus, such an enzyme may be involved in this proteolytic activation process of fungal tyrosinase (Fig. 2, *B* to *C*).

Acknowledgments—We thank E. Yamashita, A. Higashiura, M. Suzuki, and A. Nakagawa of SPring-8 BL-44XU for their support during x-ray data collection.

REFERENCES

1. Solomon, E. I., Sundaram, U. M., and Machonkin, T. E. (1996) Multicopper oxidases and oxygenases. *Chem. Rev.* **96,** 2563–2606

2. Itoh, S., and Fukuzumi, S. (2007) Monooxygenase activity of type 3 copper proteins. *Acc. Chem. Res.* **40,** 592–600
3. Flurkey, W. H., and Inlow, J. K. (2008) Proteolytic processing of polyphenol oxidase from plants and fungi. *J. Inorg. Biochem.* **102,** 2160–2170
4. Itoh, S. (2003) In *Comprehensive Coordination Chemistry II* (McCleverty, J. A., and Meyer, T. J., eds) Vol. 8, pp. 369–393, Elsevier, Amsterdam
5. van Holde, K. E., and Miller, K. I. (1995) Hemocyanins. *Adv. Protein Chem.* **47,** 1–81
6. Hazes, B., Magnus, K. A., Bonaventura, C., Bonaventura, J., Dauter, Z., Kalk, K. H., and Hol, W. G. (1993) Crystal structure of deoxygenated *Limulus polyphemus* subunit-II hemocyanin at 2.18-angstrom resolution–Clues for a mechanism for allosteric regulation. *Protein Sci.* **2,** 597–619
7. Cuff, M. E., Miller, K. I., van Holde, K. E., and Hendrickson, W. A. (1998) Crystal structure of a functional unit from octopus hemocyanin. *J. Mol. Biol.* **278,** 855–870
8. Klabunde, T., Eicken, C., Sacchettini, J. C., and Krebs, B. (1998) Crystal structure of a plant catechol oxidase containing a dicopper center. *Nat. Struct. Biol.* **5,** 1084–1090
9. Matoba, Y., Kumagai, T., Yamamoto, A., Yoshitsu, H., and Sugiyama, M. (2006) Crystallographic evidence that the dinuclear copper center of tyrosinase is flexible during catalysis. *J. Biol. Chem.* **281,** 8981–8990
10. Sendovski, M., Kanteev, M., Ben-Yosef, V. S., Adir, N., and Fishman, A. (2011) First structures of an active bacterial tyrosinase reveal copper plasticity. *J. Mol. Biol.* **405,** 227–237
11. Li, Y., Wang, Y., Jiang, H., and Deng, J. (2009) Crystal structure of *Manduca sexta* prophenol oxidase provides insights into the mechanism of type 3 copper enzymes. *Proc. Natl. Acad. Sci. U.S.A.* **106,** 17002–17006
12. Ismaya, W. T., Rozeboom, H. J., Weijn, A., Mes, J. J., Fusetti, F., Wichers, H. J., and Dijkstra, B. W. (2011) Crystal structure of *Agaricus bisporus* mushroom tyrosinase: Identity of the tetramer subunits and interaction with tropolone. *Biochemistry* **50,** 5477–5486
13. Karlin, K. D. (1993) Metalloenzymes, structural motifs, and inorganic models. *Science* **261,** 701–708
14. Gaetke, L. M., and Chow, C. K. (2003) Copper toxicity, oxidative stress, and antioxidant nutrients. *Toxicology* **189,** 147–163
15. Robinson, N. J., and Winge, D. R. (2010) Copper metallochaperones. *Annu. Rev. Biochem.* **79,** 537–562
16. Davis, A. V., and O'Halloran, T. V. (2008) A place for thioether chemistry in cellular copper ion recognition and trafficking. *Nat. Chem. Biol.* **4,** 148–151
17. Wang, N., and Hebert, D. N. (2006) Tyrosinase maturation through the mammalian secretory pathway: Bringing color to life. *Pigment Cell Res.* **19,** 3–18
18. Matoba, Y., Bando, N., Oda, K., Noda, M., Higashikawa, F., Kumagai, T., and Sugiyama, M. (2011) A molecular mechanism for copper transportation to tyrosinase that is assisted by a metallochaperone, caddie protein. *J. Biol. Chem.* **286,** 30219–30231
19. Kupper, U., Niedermann, D. M., Travaglini, G., and Lerch, K. (1989) Isolation and characterization of the tyrosinase gene from *Neurospora crassa*. *J. Biol. Chem.* **264,** 17250–17258
20. Halaouli, S., Record, E., Casalot, L., Hamdi, M., Sigoillot, J. C., Asther, M., and Lomascolo, A. (2006) Cloning and characterization of a tyrosinase gene from the white-rot fungus *Pycnoporus sanguineus*, and overproduction of the recombinant protein in *Aspergillus niger*. *Appl. Microbiol. Biotechnol.* **70,** 580–589
21. Kawamura-Konishi, Y., Tsuji, M., Hatana, S., Asanuma, M., Kakuta, D., Kawano, T., Mukouyama, E. B., Goto, H., and Suzuki, H. (2007) Purification, characterization, and molecular cloning of tyrosinase from *Pholiota nameko*. *Biosci. Biotechnol. Biochem.* **71,** 1752–1760
22. Fujieda, N., Ikeda, T., Murata, M., Yanagisawa, S., Aono, S., Ohkubo, K., Nagao, S., Ogura, T., Hirota, S., Fukuzumi, S., Nakamura, Y., Hata, Y., and Itoh, S. (2011) Post-translational His-Cys cross-linkage formation in tyrosinase induced by copper(II)-peroxo species. *J. Am. Chem. Soc.* **133,** 1180–1183
23. Fujieda, N., Murata, M., Yabuta, S., Ikeda, T., Shimokawa, C., Nakamura, Y., Hata, Y., and Itoh, S. (2012) Multifunctions of *MelB*, a fungal tyrosinase from *Aspergillus oryzae*. *ChemBioChem.* **13,** 193–201
24. Vagin, A., and Teplyakov, A. (2010) Molecular replacement with MOLREP. *Acta Crystallogr. D Biol. Crystallogr.* **66,** 22–25
25. Adams, P. D., Afonine, P. V., Bunkóczi, G., Chen, V. B., Davis, I. W., Echols, N., Headd, J. J., Hung, L. W., Kapral, G. J., Grosse-Kunstleve, R. W., McCoy, A. J., Moriarty, N. W., Oeffner, R., Read, R. J., Richardson, D. C., Richardson, J. S., Terwilliger, T. C., and Zwart, P. H. (2010) Phenix: A comprehensive python-based system for macromolecular structure solution. *Acta Crystallogr. D Biol. Crystallogr.* **66,** 213–221
26. Emsley, P., and Cowtan, K. (2004) Coot: Model-building tools for molecular graphics. *Acta Crystallogr. D Biol. Crystallogr.* **60,** 2126–2132
27. Winn, M. D., Isupov, M. N., and Murshudov, G. N. (2001) Use of TLS parameters to model anisotropic displacements in macromolecular refinement. *Acta Crystallogr. D Biol. Crystallogr.* **57,** 122–133
28. Chen, V. B., Arendall, W. B., 3rd, Headd, J. J., Keedy, D. A., Immormino, R. M., Kapral, G. J., Murray, L. W., Richardson, J. S., and Richardson, D. C. (2010) Molprobity: All-atom structure validation for macromolecular crystallography. *Acta Crystallogr. D Biol. Crystallogr.* **66,** 12–21
29. Kabsch, W., and Sander, C. (1983) Dictionary of protein secondary structure-Pattern-recognition of hydrogen-bonded and geometrical features. *Biopolymers* **22,** 2577–2637
30. Holm, L., and Rosenström, P. (2010) Dali server: Conservation mapping in 3D. *Nucleic Acids Res.* **38,** W545–W549
31. Rensing, C., and Grass, G. (2003) *Escherichia coli* mechanisms of copper homeostasis in a changing environment. *FEMS Microbiol. Rev.* **27,** 197–213
32. Yike, I. (2011) Fungal proteases and their pathophysiological effects. *Mycopathologia* **171,** 299–323